Supplementary Information

Rate-dependent structure-electrochemistry relationships and origins of capacity fading in P2-type $Na_{2/3}Fe_{2/3}Mn_{1/3}O_2$

Damian Goonetilleke,[a,†,*] Begoña Silvan,[b,c,‡] Elena Gonzalo,[b] Montserrat Galceran,[b] Montse Casas-Cabanas,[b,d] Maxim Avdeev,[e,f] Francois Fauth,[g] Teófilo Rojo,[b,h] Neeraj Sharma,[a] Damien Saurel[b,*]

[a] School of Chemistry, UNSW Sydney, Sydney NSW 2052, Australia

[b] Centre for Cooperative Research on Alternative Energies (CIC energiGUNE), Basque Research and Technology Alliance (BRTA), Alava Technology Park, Albert Einstein 48, 01510, Vitoria-Gasteiz, Spain

[c] Departamento de Física de la Materia Condensada, Facultad de Ciencia y Tecnología, Universidad del País Vasco, UPV/EHU, Apdo 644, 48080 Bilbao, Spain

[d] Ikerbasque Basque Foundation for Science, María Díaz de Haro 3, 48013, Bilbao, Spain

[e] Australian Nuclear Science and Technology Organisation, New Illawarra Road, Lucas Heights, NSW 2234, Australia

[f] School of Chemistry, The University of Sydney, Sydney, NSW 2006, Australia

[g] CELLS – ALBA Synchrotron, E-08290 Cerdanyola del Vallès, Barcelona, Spain

[h] Departamento de Química Inorgánica, Universidad del País Vasco UPV/EHU, P.O. Box. 644, 48080, Bilbao, Spain

[*] Email: damian.goonetilleke@eu.umicore.com, dsaurel@cicenergigune.com

[†] Current Affiliation: Umicore Corporate Research & Development, Watertorenstraat 33, 2250 Olen, Belgium

[‡] Current Affiliation: LiNa Energy Ltd, Unit 1 Sharpes, Mill St, South Rd, Lancaster LA1 4XQ, United Kingdom

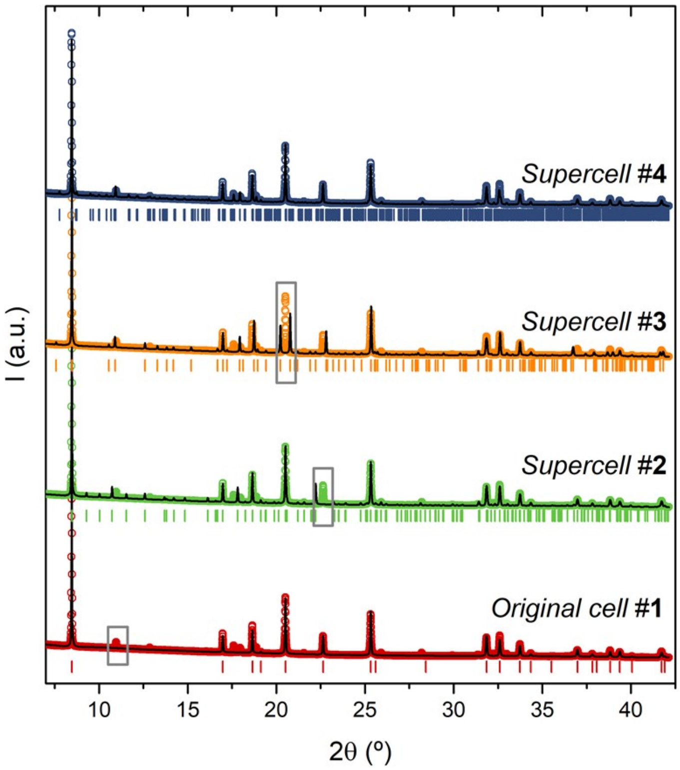

Figure S1 Le Bail refinements of P2-NFMO with different superstructures described in **Table S1**. The plane projections of these supercells are shown in **Figure S2**. Some of the reflections that are not correctly adjusted have been highlighted with grey squares.

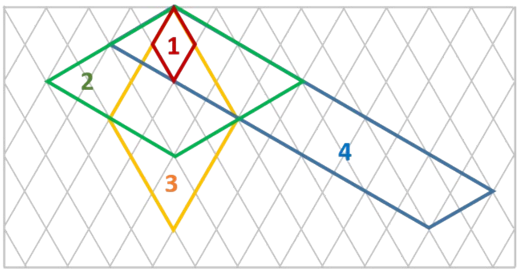

Figure S2 In-plane projection of the tested supercells. All the tested structures share the same out-of-plane stacking symmetry.

Table S1 Resulting refined parameters for the tested supercell structural models refined against the SXRD pattern of P2-NFMO (**Figure 1a**). All the cells share the same stacking order. The cell 1 is the original P2 structure. Cells 2 and 3 are defined with a hexagonal base (see **Figure S2**), where cell 2 has been taken from the literature,[92] and cell 3 corresponds to three times per side in *a* and *b* directions. The supercell 4 has been chosen using DICVOL software and is defined with a rotated monoclinic space group.

Cell #	**S.G.**	**a / Å**	**b / Å**	**c / Å**	**α / °**	**β / °**	**g / °**
1	$P6_3/mmc$	$a_0 = 2.94$	a_0	$c_0 = 11.18$	90	90	120
2	$P6_3/mmc$	$2\sqrt{3}a_0$	$2\sqrt{3}a_0$	c_0	90	90	120
3	$P6_3/mmc$	$3a_0$	$3a_0$	c_0	90	90	120
4	Pm	$5\sqrt{3}a_0$	c_0	$\sqrt{3}a_0$	90	120	90

Magnetic measurements

The inverse susceptibility measurements are presented in **Figure S3**, and the magnetization versus DC magnetic field at 2.5 K is shown as an inset. A linear behaviour of the inverse susceptibility is observed in the range 180 - 300 K, in agreement with the Curie-Weiss law:

$$\chi^{-1} = \frac{T + \theta}{C} \quad (1)$$

where θ is the Weiss constant and *C* is the Curie constant, which is defined as:

$$C = \frac{N_A {\mu_{eff}}^2 {\mu_B}^2}{3k_B} \quad (2)$$

where N_A is the Avogadro's number, μ_{eff} the effective moment, μ_B the Bohr's magneton and k_B the Boltzmann's constant. The effective moment μ_{eff} and Weiss temperature θ deduced from the fit of the inverse susceptibility presented in **Figure S3** using **Equation 2** is shown in **Table S2**. P2-NFMFO exhibits an effective magnetic moment near room temperature of about 5.11, which is close to the theoretical value of 5.32 when high spin (HS) Fe^{III} (*S* = 2.5) and HS Mn^{IV} (*S* = 1.5) are considered assuming the Landé factor g = 2:

$$\mu_{eff} = g\sqrt{S(S+1)} \quad (3)$$

$$\mu^{NMFO}_{eff} = \sqrt{\frac{2}{3}\left(\mu^{Fe(III)}_{eff}\right)^2 + \frac{1}{3}\left(\mu^{Mn(IV)}_{eff}\right)^2} \quad (4)$$

Moreover, the negative root of the linear fits with Equation 1 near room temperature, corresponding to a large negative Weiss constant θ = -130 K which indicates strong antiferromagnetic coupling. The non-linear behaviour below ≈ 150 K can be attributed to increasing local magnetic correlations and competing Mn^{IV}-Fe^{III} ferro- and Fe^{III}-Fe^{III}-antiferromagnetic interactions.[93]

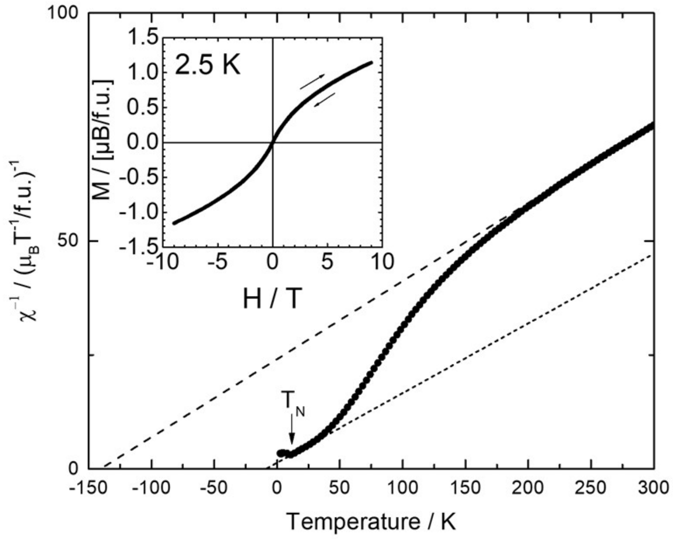

Figure S3 Inverse susceptibility of the P2-NFMO material, together with the linear fit using Equation 1 in the range 200-300 K. Inset: Magnetization versus DC magnetic field at 2.5 K.

Table S2 Effective moment μ_{eff} and Weiss temperature θ deduced from the linear fit of the inverse susceptibility measurement (**Figure S3**) near room temperature (high temperature) and near Néel temperature (low temperature).

μ_{eff}	θ / K	T_N / K
5.107 ± 0.007	-141 ± 2	8.1

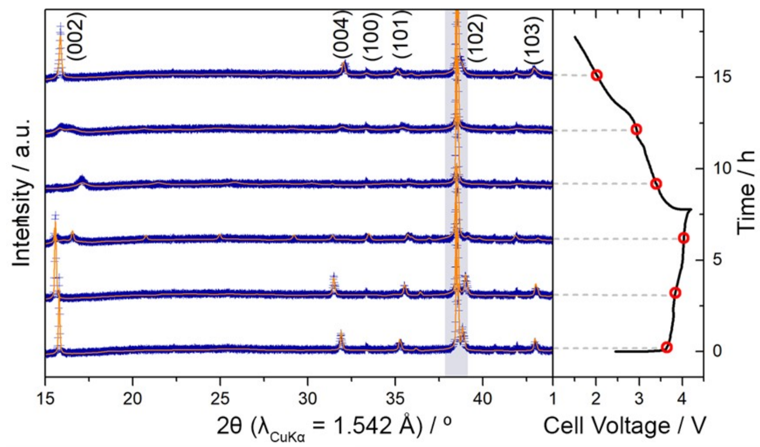

Figure S4 Selected Le Bail refinements of low-rate operando XRD data collected from P2.

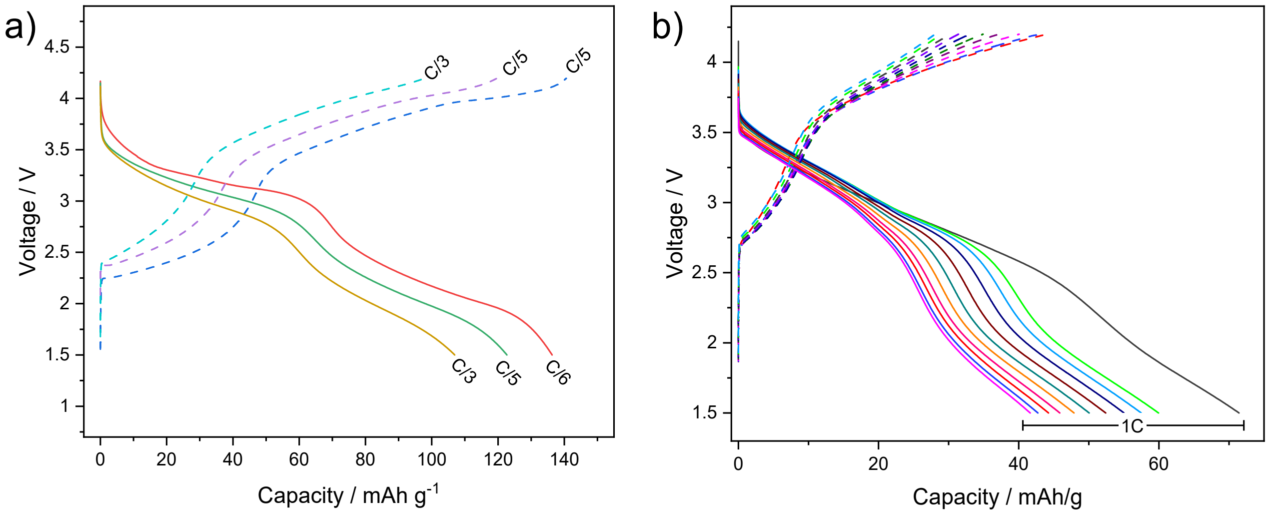

Figure S5 Voltage versus capacity curves delivered by the P2-type cell during *operando* cycling at a) moderate and b) high current densities.

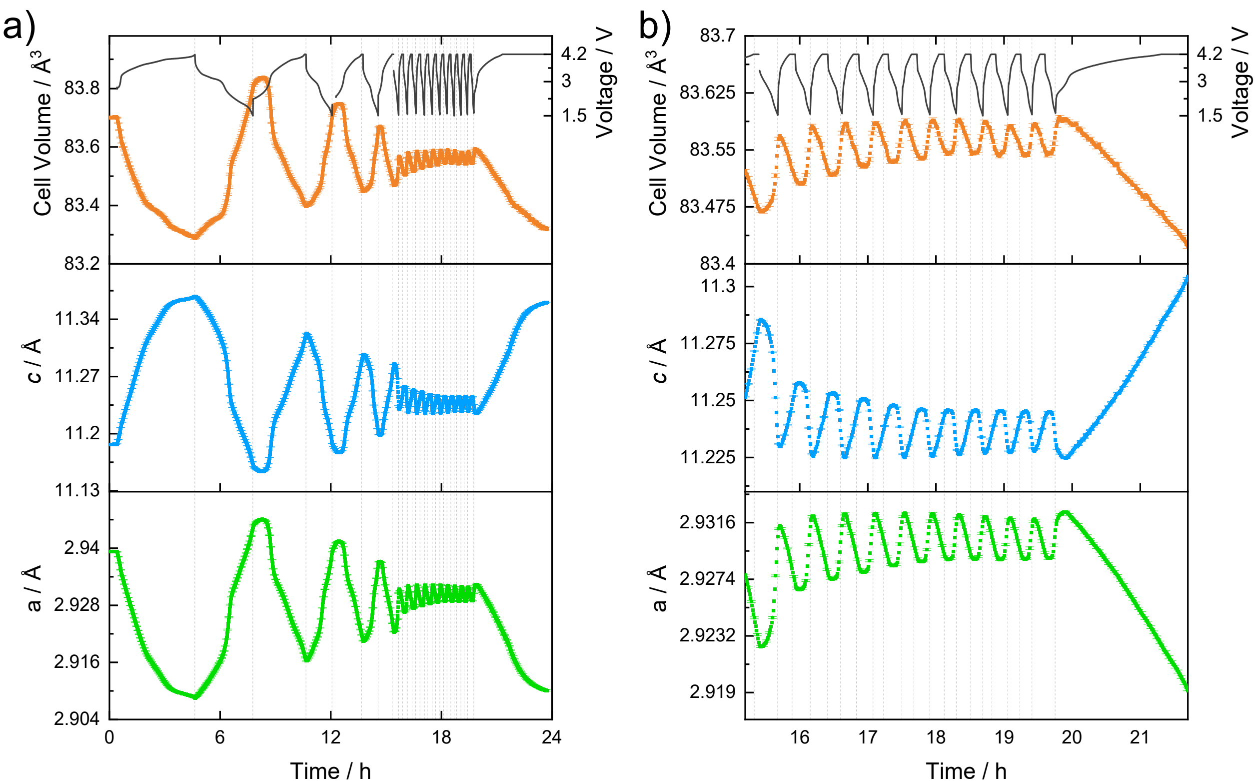

Figure S6 Refined lattice parameters of P2-NFMO determined from SXRD data collected during the high-rate *operando* SXRD cycling experiment at a) moderate and b) high current densities.

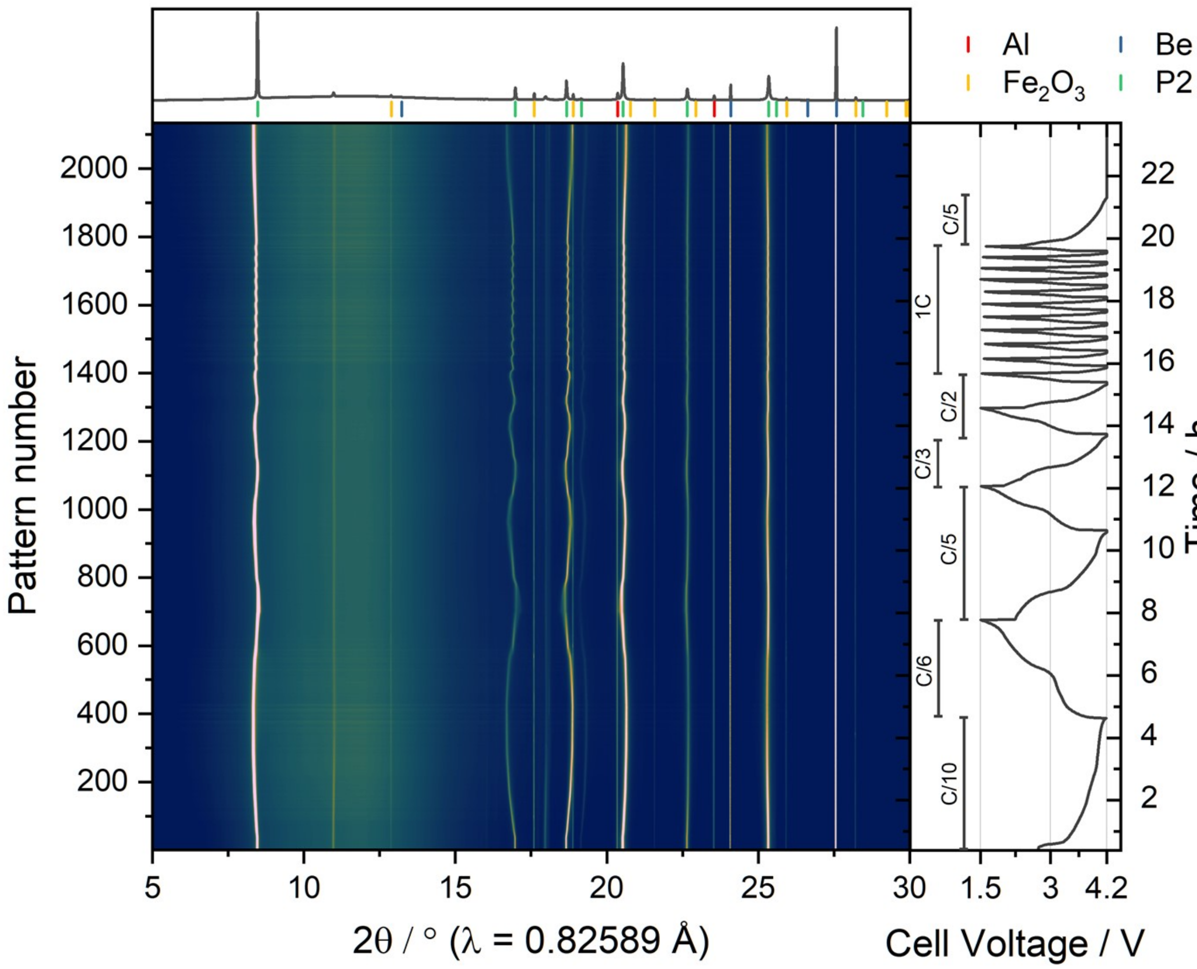

Figure S7 *Operando* SXRD data collected during cycling of the P2-NFMO containing cell.

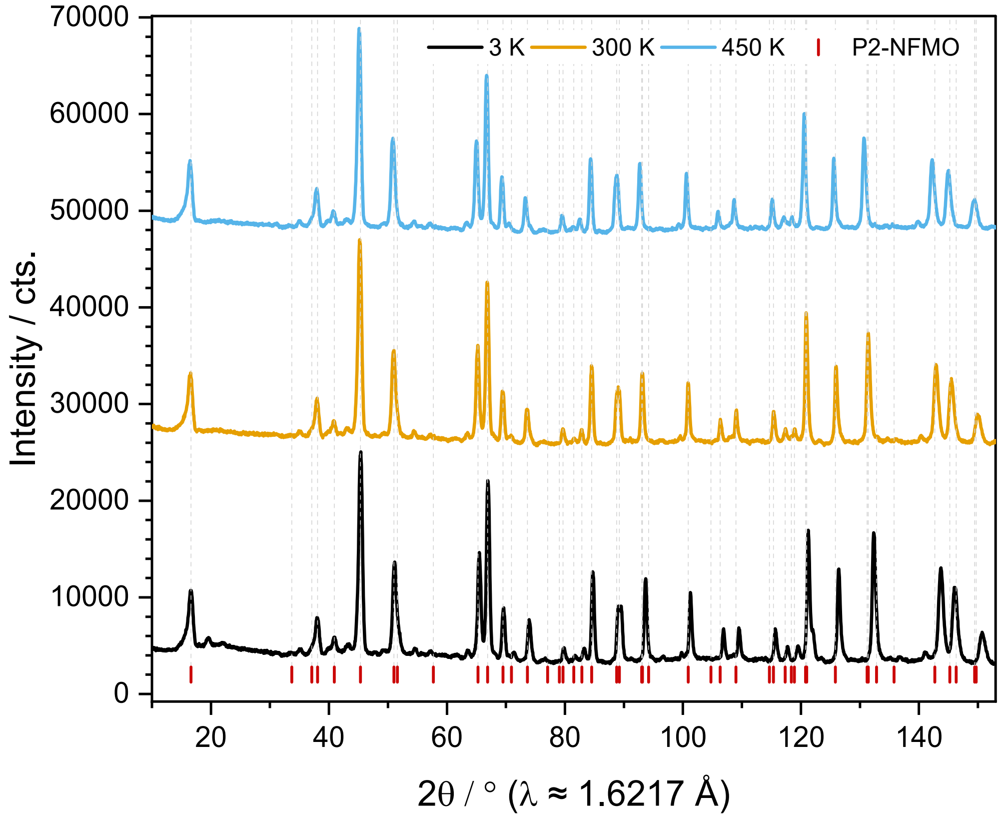

Figure S8 Neutron diffraction patterns collected from P2-NFMO at various temperatures.

Table S3 Refined structural parameters of P2-NFMO determined from neutron diffraction patterns shown in **Figure S7**, collected at various temperatures.

Temperature / K	*a* / Å	*c* / Å	Vol / Å³	z_O	Na(1) SOF	Na(2) SOF
3	2.93871(12)	11.12758(41)	83.223(6)	0.09358(16)	0.133(9)	0.534(9)
300	2.94318(9)	11.18267(25)	83.890(4)	0.09289(10)	0.136(7)	0.552(8)
450	2.94761(14)	11.22524(49)	84.463(7)	0.09296(17)	0.117(9)	0.550(9)